Journal of Magnetic Resonance **140,** 162–171 (1999)
Article ID jmre.1999.1838, available online at http://www.idealibrary.com on IDEAL®

Functional MR Imaging of the Human Brain Using FLASH: Influence of Various Imaging Parameters

Christine Preibisch*,† and Axel Haase*

*Physikalisches Institut, Experimentelle Physik V, Universität Würzburg, 97074 Würzburg; and †Institut für Röntgendiagnostik, Abteilung für Neuroradiologie, Universität Würzburg, 97080 Würzburg, Germany

Received December 18, 1998

In this study the influence of a large variety of imaging parameters on the signal increase (ΔS) and the contrast-to-noise ratio (CNR) of functional magnetic resonance imaging experiments was determined using FLASH imaging at 2 T. During visual stimulation of the brain we detected significant variations of ΔS as a function of the echo time (30 ms: 3.5 ± 0.4%, 60 ms: 6.8 ± 0.7%), slice thickness (2.5 mm: 6.8 ± 0.7%, 10.0 mm: 3.3 ± 0.3%), and pixel size (4.69 mm: 3.1 ± 0.3%, 1.88 mm: 5.9 ± 0.5%). Significant changes of ΔS with flip angle occurred for TE = 20 ms (15°: 2.1 ± 0.2%, 60°: 3.2 ± 0.5%). At TE = 30 ms there still was a slight increase (15°: 3.0 ± 0.4%, 60°: 3.8 ± 0.5%), while at TE = 50 ms no changes of ΔS could be detected with flip angle. Furthermore, ΔS decreased with the use of first-order flow and motion compensation (off: 5.8 ± 0.6%, on: 4.5 ± 0.5%). The purpose of this study was to identify the optimal imaging parameters for blood oxygenation level dependent contrast using FLASH imaging at 2 T. Relying on a time normalized contrast-to-noise ratio (CNR^n) we found the following parameters to be optimal: TE ≈ 40–50 ms, a rather low spatial resolution (slice thickness ≈ 5.0–7.5 mm, pixel size ≈ 2.3–4.6 mm, matrix size 64 × 48), and flip angles lower than 30°. Flow compensation should not be applied, and a rather low bandwidth of ≈2.5 kHz is favorable, as it yields a superior signal-to-noise ratio.

Key Words: **fMRI; FLASH; CNR; imaging parameters.**

INTRODUCTION

Since the first functional magnetic resonance imaging (fMRI) experiments had been conducted (*1, 2*), it is well known that the results are very sensitive to the imaging parameters (*3*). The observed signal changes are mainly due to alterations in blood oxygenation (blood oxygenation level dependent (BOLD) effect) (*4–6*), since the increase in blood flow by far exceeds the physiological oxygen demand (*5, 7*). Observed signal changes depend on echo time (*5, 8*), field strength (*3, 5, 9–11*), spatial resolution (*12–14*), and various other parameters (*14, 15*) as well as on the imaging sequence used. A large variety of studies were performed in order to characterize different features of BOLD imaging depending on physiological properties as well as on physical properties of the imaging sequences (*11, 15–20*). In a restricted experiment time, activation can only be detected if the signal increase due to activation exceeds the baseline signal fluctuations due to noise. The time normalized contrast-to-noise ratio (CNR^n), i.e., the ratio of the signal increase and the standard deviation of random signal fluctuations, normalized by the square root of the acquisition time, can thus be used as a quantitative measure for the quality of a fMRI experiment.

The purpose of this study was to experimentally determine the optimal values for a large variety of imaging parameters with respect to the signal increase and the noise characteristic of FLASH imaging at 2 Tesla.

SUBJECTS AND METHODS

MR Methods

Functional imaging was performed on a 2.0 T Bruker TOMIKON S200 Spectrometer (Bruker Medizintechnik, Ettlingen, Germany) using the body coil for excitation and a linear receive-only head coil for signal detection. Eight healthy volunteers (two women, six men, ages 25 to 35) were the subjects of the study. Written informed consent was obtained from all subjects prior to investigation. Foam pads were used to minimize head movement during examinations.

Visual stimulation was performed using homebuilt goggles emitting red light. The stimulation paradigm consisted of three periods of darkness alternating with a red light flashing at 8 Hz (*20, 21*). For each subject up to 30 fMRI experiments were performed with different imaging parameters. The duration of a single experiment was always limited to about 4 min. This is why not all experiments were conducted with the same number of images (NI). Depending on the acquisition time for 1 image, 6, 10, or 20 images were collected per on/off period, which resulted in a total NI of 18, 30, or 60 per experiment. The experiments were always conducted in the same succession. However, for each subject, the full set of experiments was split up individually into two or three sessions of about 1.5 to 2 h on different days, to limit the fatigue of the subjects.

1090-7807/99 $30.00

Imaging Protocol

First, a set of three orthogonal scout images (sagittal, coronal, and axial) and 15 high-resolution T_1-weighted sagittal images were acquired in order to localize the appropriate plane for the functional imaging study. One oblique slice was then placed along the calcarine cortex. Volume-selective shimming of a 10-cm-thick axial slice centered around the visual cortex was performed for each subject.

In preliminary experiments, appropriate parameters of a T_2^*-weighted FLASH sequence were determined which yielded reliable activation in several subjects. This basic sequence was then repeated in every session for each subject. The parameters for the basic sequence were chosen as follows: TE = 50 ms, TR = 83 ms, flip angle (FA) 15°, Gaussian excitation pulse with pulse length 900 μs, pixel size 2.34 mm (rectangular FOV 30 × 22.5 cm and matrix 128 × 96), slice thickness (ST) 5 mm. An extremely low bandwidth (BW) of 2.5 kHz was used because it provided the highest possible SNR with a minimal TE of 30 ms. The sequence contained RF spoiling, but no flow compensation (first-order flow and motion compensated gradient waveforms in read and slice encoding direction). The acquisition time for one image (T_{acq}) was 8 s in this case, thus a total of 30 images could be acquired in about 4 min. This sequence was then used as a basis, from which all variations were derived. The basic parameters were chosen to allow the parameters to be varied one by one, keeping the remaining basic parameters constant. The final protocol consisted of 10 subsets of experiments, where the following parameters were varied independently:

- TE from 30 to 60 ms (for TE 60 ms: TR 93 ms/T_{acq} 9 s)
- FA from 15 to 60° at different echo and repetition times:
  - -TE 20 ms/TR 40 ms/T_{acq} 4 s/NI 60
  - -TE 30 ms/TR 63 ms/T_{acq} 7 s/NI 30
  - -TE 50 ms/TR 83 ms, RF spoiled
  - -TE 50 ms/TR 83 ms, phase rewinded
- ST from 2.5 to 10 mm
- pixel sizes from 1.17 to 4.69 mm:
  - -FOV from 24.0 to 30.0 cm (matrix size 128 × 96)
  - -matrix size from 64 to 256 (FOV 30.0 cm):
    - 64 × 48: T_{acq} 4 s/NI 60
    - 256 × 192: TE 55.4 ms/TR 113 ms/T_{acq} 22 s/NI 18
- BW from 2.5 to 15.0 kHz
- flow compensation on/off.

Unless stated otherwise, TE was 50 ms, TR 83 ms, FA 15°, FOV 30 × 22.5 cm, matrix 128 × 96, ST 5 mm, BW 2.5 kHz, T_{acq} 8 s, NI 30.

Analysis

The data analysis was performed on an external Silicon Graphics Indy workstation. Minimum head movement was verified by playing the images through a cine loop. A whole subset of experiments of a subject was discarded if at least one experiment showed severe motion artifacts. In order to allow a steady state to be established the very first point in each experiment was excluded from evaluation. Since the signal time course is governed by the delayed hemodynamic response (*22, 23*) to the stimulation paradigm, the first point of each period was discarded with NI = 18 or NI = 30; with NI = 60 the first two points were discarded. This means that the signal averages in rest $\langle S_{rest}(t)\rangle$ resp. active state $\langle S_{act}(t)\rangle$ were calculated in the steady-state regions of the signal time course. For statistical evaluation, correlation with a boxcar reference function was computed with AFNI (R. Cox, Medical College of Wisconsin). A level of significance of $P \leq 0.002$, corresponding to threshold values for the correlation coefficient of $r_{th} = 0.8$ for NI = 18, $r_{th} = 0.6$ for NI = 30, and $r_{th} = 0.44$ for NI = 60 was used. Each pixel with correlation coefficient $r > r_{th}$ inside the visual cortex was counted as activated (N_{act}), and the relative signal increase,

$$\Delta S_{pix} = \frac{\langle S_{act}(t)\rangle - \langle S_{rest}(t)\rangle}{\langle S_{rest}(t)\rangle}, \quad [1]$$

during activation was computed. For comparison of the different parameter settings the mean signal increase over subjects,

$$\Delta S = \frac{\Sigma_n \langle \Delta S_{pix}\rangle}{n}, \quad [2]$$

was computed, where $\langle \Delta S_{pix}\rangle = \Sigma_{pix}\, \Delta S_{pix}/N_{act}$ is the mean signal increase for a single subject, and n denotes the number of subjects included for evaluation.

For the calculation of the contrast-to-noise ratio of the experiments an estimate of the baseline fluctuations was also needed. However, the global signal-to-noise ratio (*24*),

$$SNR = \frac{\langle S(x, y)\rangle}{\sigma_N \cdot 1.5}, \quad [3]$$

with the average signal in a region of interest (ROI) inside $\langle S(x,y)\rangle$ and the standard deviation of noise in a ROI outside of the brain σ_N, only gives a lower limit for the magnitude of the baseline fluctuations, since it is not sensitive to time-course variations caused by physiologic processes, artifacts, or system instabilities. Therefore,

$$SNR_{pix} = \frac{\langle S(t)\rangle}{\sigma(S(t))}, \quad [4]$$

with the average time-course signal $\langle S(t)\rangle$ and the activation-independent standard deviation,

$$\sigma(S(t)) = \sqrt{\frac{\Sigma(S_{\text{rest}}(t) - \langle S_{\text{rest}}(t)\rangle)^2 + \Sigma(S_{\text{act}}(t) - \langle S_{\text{act}}(t)\rangle)^2}{2m - 1}}, \quad [5]$$

was determined as a measure of time-course fluctuations, where m denotes the number of time points in rest resp. activated state which were used for the calculation of the time averages and standard deviation.

On the basis of these quantities CNR was calculated, which can be generally defined as the ratio of the relative signal increase ΔS and the magnitude of time-course fluctuations δS (*20*). Since the relative magnitude of time-course fluctuations can be considered the reciprocal value of SNR,

$$\text{CNR} = \frac{\Delta S}{\delta S} = \Delta S \cdot \text{SNR}. \quad [6]$$

In order to take into account the influence of any possible pixel time-course instability,

$$\text{CNR}_{\text{pix}} = \langle \Delta S_{\text{pix}} \cdot \text{SNR}_{\text{pix}} \rangle = \frac{\Sigma_{\text{pix}}(\Delta S_{\text{pix}} \cdot \text{SNR}_{\text{pix}})}{N_{\text{act}}} \quad [7]$$

was calculated. Finally, CNR_{pix} was averaged over all included subjects. For comparison, we also determined the global

$$\text{CNR} = \Delta S \cdot \text{SNR}_{\text{rel}} = \Delta S \cdot \frac{\Sigma_n \text{SNR}/\text{SNR}_{\text{base}}}{n}, \quad [8]$$

which gives the highest possible CNR in the absence of additional time-course fluctuations, where SNR_{rel} is the SNR of the first image of the corresponding experiment compared to the basic experiment (SNR_{base}) averaged over n subjects. Since the measurement time is an essential factor in fMRI we finally determined a time-normalized CNR^n resp. $\text{CNR}^n_{\text{pix}}$. As shorter measurement times allow for averaging, where SNR increases with the square root of the acquisition time, we calculated these quantities as

$$\text{CNR}^n = \frac{\text{CNR}}{\sqrt{T_{\text{acq}}}} \quad \text{and} \quad \text{CNR}^n_{\text{pix}} = \frac{\text{CNR}_{\text{pix}}}{\sqrt{T_{\text{acq}}}}. \quad [9]$$

RESULTS

Influence on ΔS

Figure 1 shows the variation of ΔS including those parameters where significant changes occurred. ΔS increased with echo time from 3.5 ± 0.4% at 30 ms to 6.8 ± 0.7% at 60 ms and decreased with slice thickness from 6.8 ± 0.7% at 2.5 mm to 3.3 ± 0.3% at 10 mm. The variation of ΔS with pixel size ranged from 3.1 ± 0.3% at 4.69 mm (64 matrix, FOV 30 cm) to 5.9 ± 0.5% at 1.88 mm (128 matrix, FOV 24 cm). These changes were mainly caused by the different matrix sizes; the moderate changes in FOV did merely influence ΔS. At 1.17 mm (256 matrix, FOV 30 cm) no signal change could be determined, since only a single subject showed significant activation with this matrix size. This was obviously caused by the rather low SNR and the small number of images per experiment. With different flip angles, a significant increase of ΔS could only be detected for TE 20 ms/TR 40 ms, where ΔS increased from 2.1 ± 0.2% at 15° to 3.2 ± 0.5% at 60°. For TE 30 ms/TR 63 ms, ΔS still showed a tendency to rise from 3.0 ± 0.4% at 15° to 3.8 ± 0.5% at 60°; at TE 50 ms/TR 83 ms, however, no variation could be detected with spoiled and rewinded FLASH. Application of flow compensation led to a decrease of ΔS from 5.8 ± 0.6% without to 4.5 ± 0.5% with flow compensation.

Influence on CNR^n and CNR^n_{pix}

Generally, we found SNR_{pix} to be about half the value of SNR. The subject average of the SNR of the basic experiment was 90 ± 10, whereas the corresponding SNR_{pix} was 42 ± 8. CNR^n and $\text{CNR}^n_{\text{pix}}$ averaged over subjects are shown in Figs. 2 to 6. $\text{CNR}^n_{\text{pix}}$ is at least a factor of 2 lower than CNR^n, and it decreases faster toward unfavorable imaging conditions. Figure 2 shows the dependence of CNR^n and $\text{CNR}^n_{\text{pix}}$ on the echo time. One can see that CNR^n continuously rises toward an echo time of 60 ms, whereas $\text{CNR}^n_{\text{pix}}$ declines and shows a flat peak at about 40–50 ms. This implies that the optimal TE lies somewhat below T_2^*, as independent measurements in three different subjects consistently yielded a T_2^* of about 60 ms in the visual cortex.

For slice thickness (Figs. 3a and 3b), both curves show a clear maximum at ≈5.0–7.5 mm, where CNR^n tends to the higher and $\text{CNR}^n_{\text{pix}}$ to the lower value. CNR^n and $\text{CNR}^n_{\text{pix}}$ also show a distinct dependence on pixel size (Figs. 3d and 3e). While CNR^n steadily increases for pixel sizes between 1.88 and 4.69 mm, $\text{CNR}^n_{\text{pix}}$ remains rather constant over the whole range.

For experiments with different flip angles, the distinct behavior of CNR^n and $\text{CNR}^n_{\text{pix}}$ is most likely due to flow artifacts which deteriorate image quality at higher flip angles. At echo times of 20 and 30 ms the peak values of $\text{CNR}^n_{\text{pix}}$ seem to be shifted slightly toward lower flip angles compared to CNR^n (Fig. 4). For a TE of 50 ms (spoiled and rewinded FLASH), $\text{CNR}^n_{\text{pix}}$ even drops off for flip angles higher than 15° (Fig. 5). Hence, flip angles lower than 30° seem to be optimal for fMRI experiments, even though CNR^n peaks for flip angles between 30 and 45°. The results for spoiled and rewinded FLASH at TE = 50 ms are rather similar for flip angles between 30 and 60°. However, ΔS, CNR^n, and even $\text{CNR}^n_{\text{pix}}$ clearly show higher values for rewinded FLASH.

As far as bandwidth is concerned, one can see in Figs. 6a and 6b that CNR^n and $\text{CNR}^n_{\text{pix}}$ decrease rapidly toward higher BW. The increase of $\text{CNR}^n_{\text{pix}}$ at a BW of 15 kHz is most likely artifactual because of low SNR (see discussion below). Application of flow compensation seemed to reduce the contrast-to-noise ratio since both CNR^n and $\text{CNR}^n_{\text{pix}}$ tended to be higher

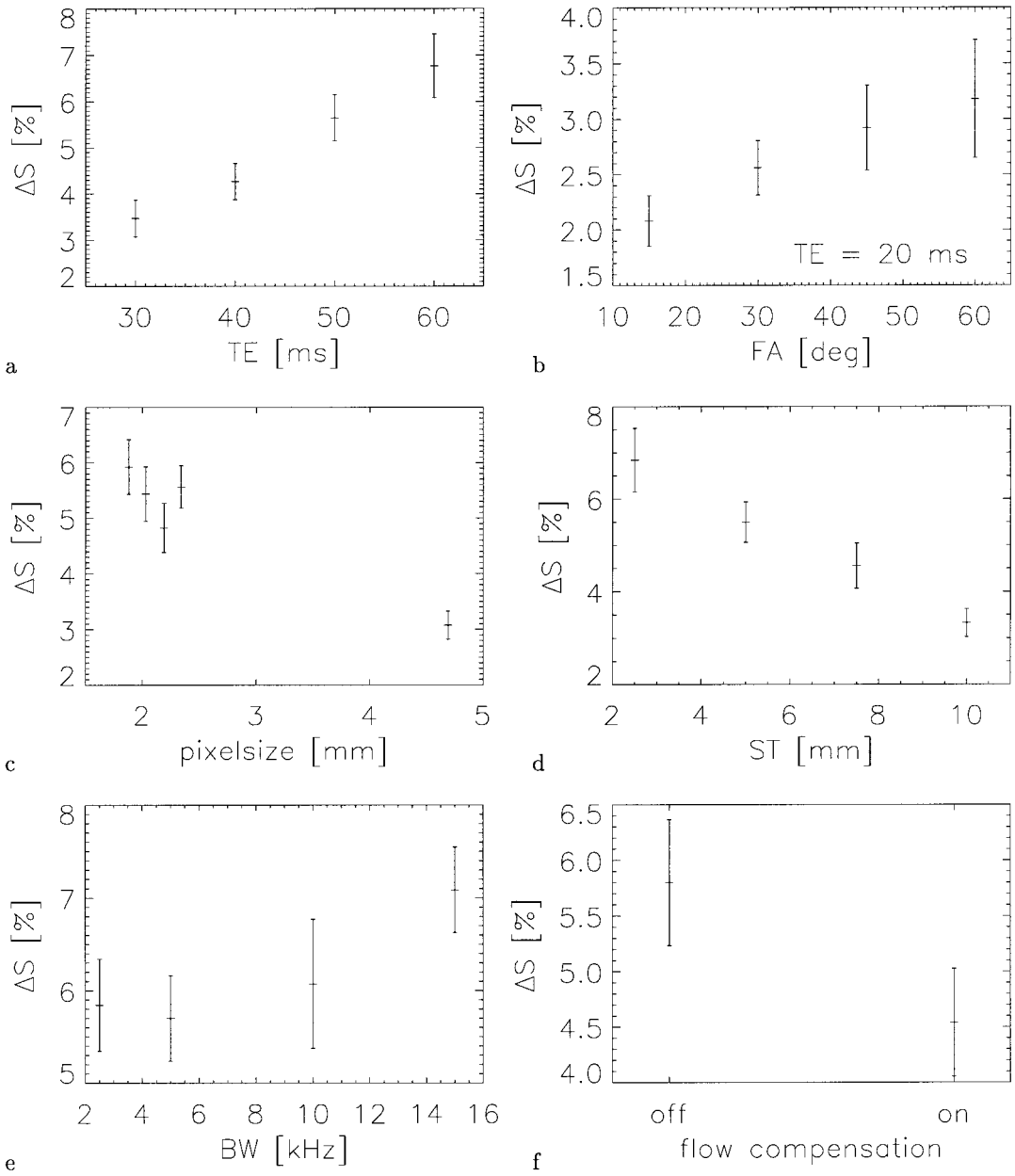

FIG. 1. Signal increase ΔS depending on (a) echo time ($n = 6$), (b) flip angle at TE = 20 ms ($n = 5$), (c) pixel size ($n = 8$), (d) slice thickness ($n = 7$), (e) bandwidth ($n = 7$), and (f) flow compensation ($n = 5$). The error bars indicate the standard error over n subjects.

without flow compensation (Figs. 6d and 6e). This is obviously due to the reduced ΔS, since the SNR was slightly higher with flow compensation.

Influence on N_{act}

Generally, the number of activated pixels largely varied over subjects and conditions. However, in Figs. 2 to 6 one can see that the subject average of N_{act} closely resembles the behavior of CNR^n, and especially of CNR^n_{pix}. One exception is the dependence on pixels size where the activated area $N_{act} \cdot (A/A_{base})$ increased together with CNR^n toward 4.69 mm (Figs. 3d–3f). The other exception is the dependence on BW, where CNR^n_{pix} shows an increase at BW 15 kHz, while CNR^n and N_{act} consistently decrease toward a higher bandwidth (Figs. 6a–6c).

DISCUSSION

Influence of Echo Time

In agreement with the literature (*8, 9, 14*), we found a linear increase of ΔS with echo time. As expected due to the field

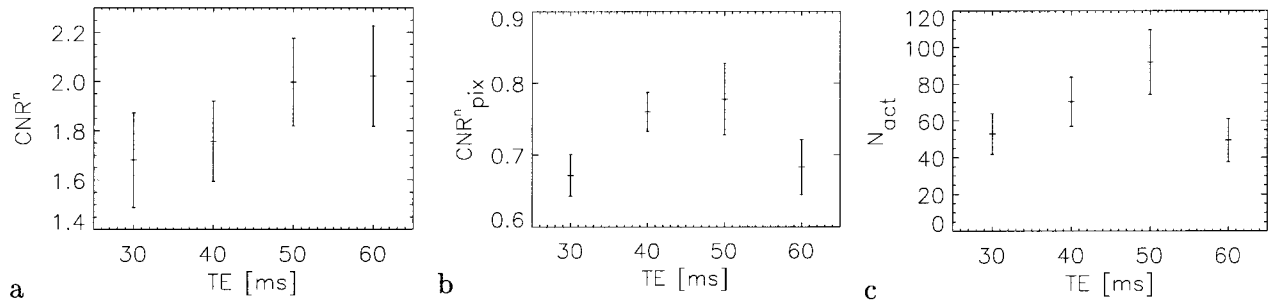

FIG. 2. (a) CNR^n, (b) CNR^n_{pix}, and (c) N_{act} depending on echo time ($n = 6$). The error bars indicate the standard error over n subjects.

strength dependence of the BOLD contrast (*5, 11*), the signal changes from 3.5 ± 0.4% at 30 ms to 6.8 ± 0.7% at 60 ms lie well between signal changes reported by other groups at higher and lower field strengths. At 4 T, Menon *et al.* (*8*) found an increase in signal from ≈2.5% at 10 ms to ≈13% at 60 ms (≈7% at 30 ms). At 1.5 T, Thompson *et al.* (*14*) reported an increase from ≈0.7% at TE = 10 ms to ≈1.6% at TE = 30 ms. At echo times higher than 38 ms this group found a high intersubject variability, which could be due to an insufficient shim in the clinical environment. Gati *et al.* (*11*) investigated the field strength dependence of ΔS and found for TE = T_2^* (88 ms, 69 ms, 32 ms) 13.3 ± 2.3, 18.4 ± 4.0, and 15.1 ± 1.2% for large vessels, and 1.4 ± 0.7, 1.9 ± 0.7, and 3.3 ± 0.2% in tissue at 0.5, 1.5, and 4 T, respectively. From this, in combination with SNR measurements, they concluded that the CNR increase in tissue is stronger, while that in vessels is less than linear with field strength. According to the literature, the CNR of any BOLD contrast experiment should be optimal for TE = T_2^*, since the absolute signal increase shows a maximum at that time (*8, 11, 20*). However, this is only true if noise does not increase with echo time. In this study we found a maximum CNR^n_{pix} at ≈40–50 ms, while CNR^n continued to rise up to the maximal TE = 60 ms. Since the measurement of T_2^*, in three different subjects consistently yielded a value of about 60 ms, we concluded that the optimal value for TE lies somewhat below T_2^*. Similar results were also found by Frahm *et al.* (*12*), who also measured a T_2^* of about 60 ms at 2 T and concluded that TE ≈ 30–40 ms is a good compromise between good oxygenation sensitivity and SNR. This distinct behavior of CNR^n and CNR^n_{pix} reveals that the decrease in SNR_{pix} with TE is substantially stronger than the decrease of SNR. One explanation is that the observed signal changes are partly

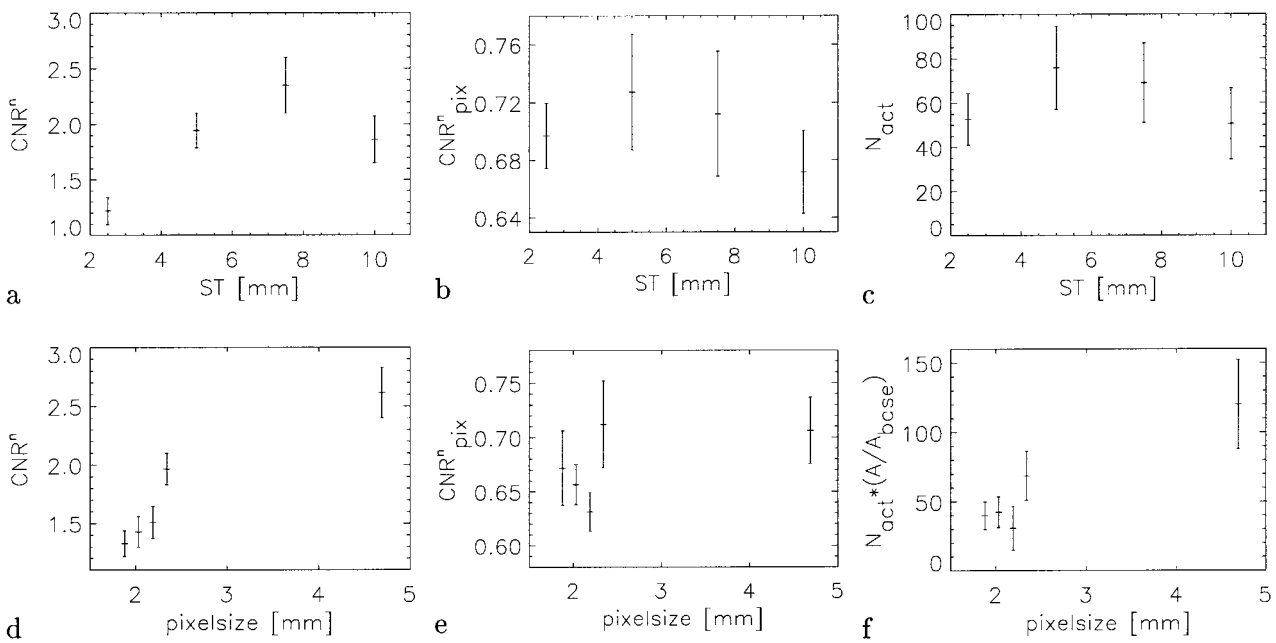

FIG. 3. Dependence of CNR^n, CNR^n_{pix}, and N_{act} on (a–c) slice thickness ($n = 7$) and (d–f) pixel size ($n = 8$). In (f) N_{act} is corrected for the different pixel sizes by multiplication with the ratio A/A_{base}, where A is the area of the respective pixel and A_{base} is the area for the basic pixel size 2.34 mm. The error bars indicate the standard error over n subjects.

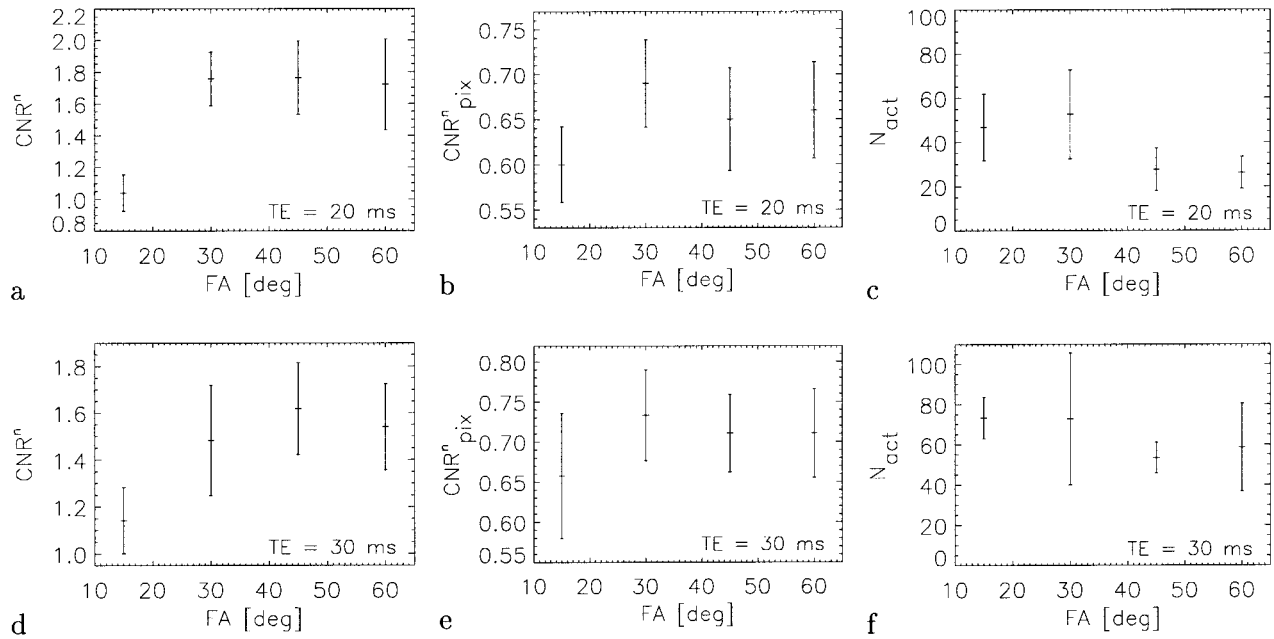

FIG. 4. Dependence of CNR^n, CNR^n_{pix}, and N_{act} on flip angle: (a–c) TE = 20 ms ($n = 5$); (d–f) TE = 30 ms ($n = 5$). The error bars indicate the standard error over n subjects.

caused by pixels near larger venules, which show a lower T_2^* (*8, 11*) and thus also a lower optimal TE. However, it cannot be excluded that T_2^* was lower than 60 ms in individual subjects, as this parameter was not determined in any case.

Influence of Spatial Resolution

Our finding of increased signal changes with increased spatial resolution is in agreement with the concept of reduced partial volume effects. Frahm *et al.* (*12*) found the signal

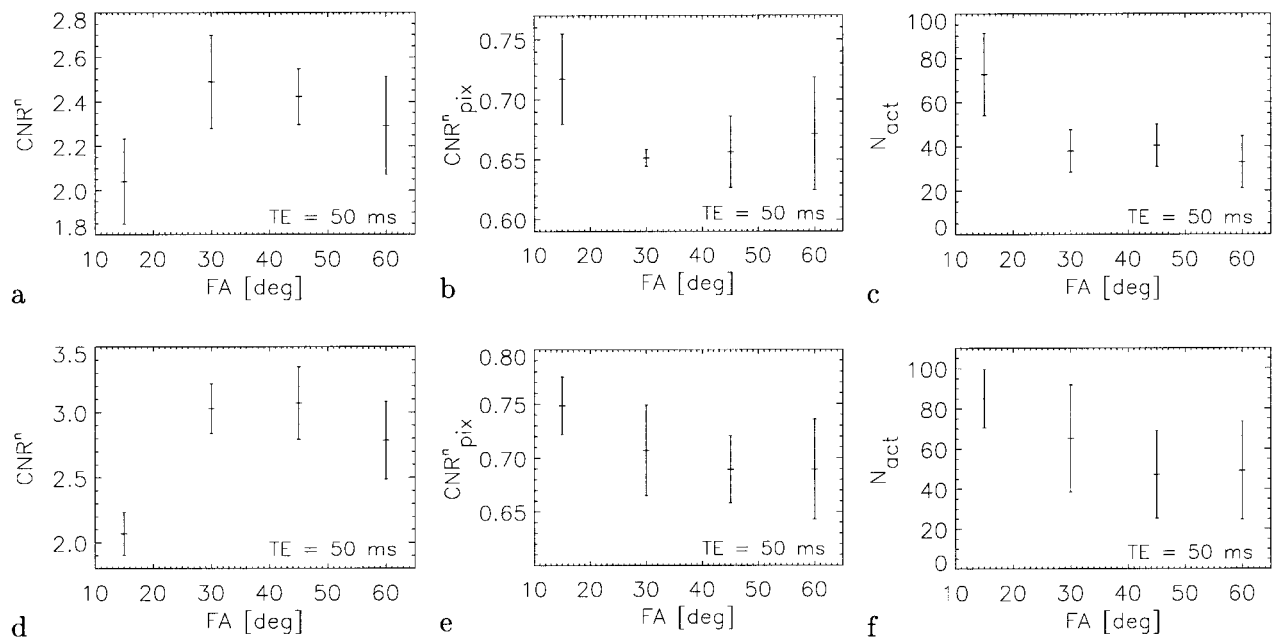

FIG. 5. Dependence of CNR^n, CNR^n_{pix}, and N_{act} on flip angle: (a–c) TE = 50 ms, RF spoiled ($n = 7$); (d–f) TE = 50 ms, phase rewinded ($n = 6$). The error bars indicate the standard error over n subjects.

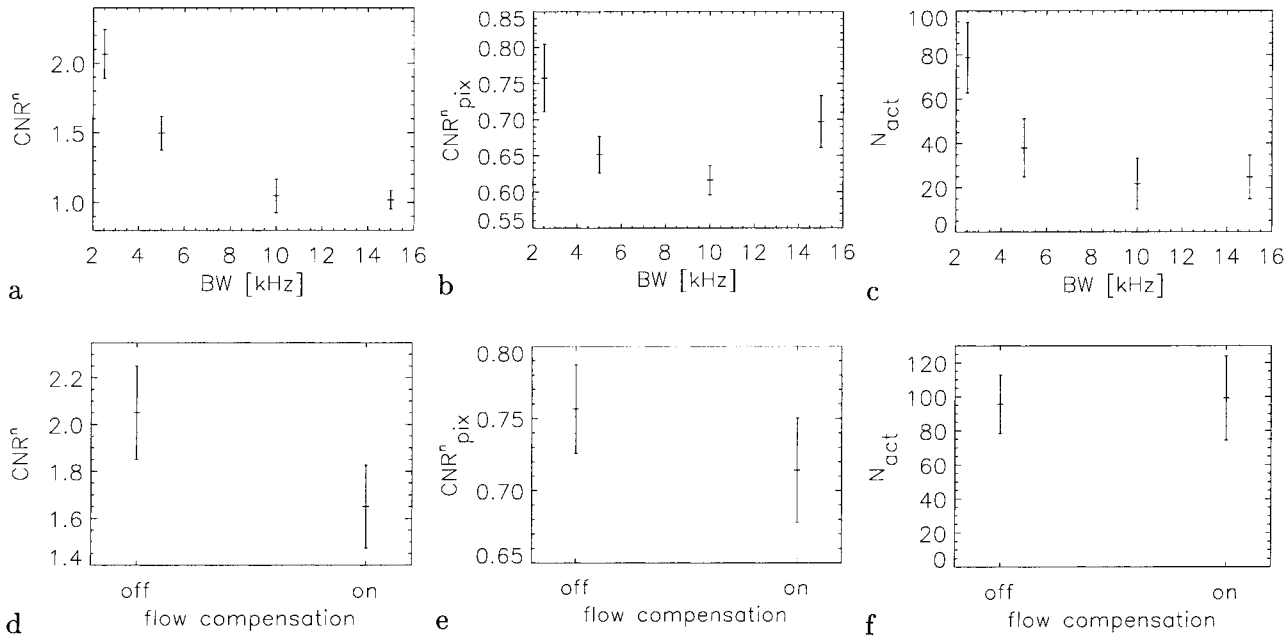

FIG. 6. Dependence of CNR^n, CNR^n_{pix}, and N_{act} on (a–c) bandwidth ($n = 7$) and (d–f) flow compensation ($n = 5$). The error bars indicate the standard error over n subjects.

increase to rise to twice its original value when reducing the slice thickness by 50%; an equal reduction in matrix size for identical ROIs did not show an effect on the observed signal change. Lai *et al.* (*13*) detected high focal signal changes with increased spatial resolution, suggesting macrovasculature to be involved (*13*). Thompson *et al.* (*14*) also found an increased signal change with reduced slice thickness (≈1.5% at 10 mm, ≈2.8% at 3 mm) but their finding of increased signal change with increased FOV is inconsistent with the other studies. In the present study we found no significant variation of the signal change with FOV, whereas doubling of matrix size and reduction of slice thickness significantly increased the observed ΔS. The increase of CNR^n at pixel size 4.69 mm (64 matrix) is solely due to the reduced scan time. Without consideration of the measurement time CNR is about constant for the matrix sizes 64×48 and 128×96, as the decrease of SNR and the increase in ΔS nearly compensate each other. Taking into account the increase in the size of the activated area we can conclude that it would be favorable to use a reduced matrix size in concert with a rather small FOV, as the decrease in SNR with FOV reduction can easily be compensated by a higher number of images.

Influence of Flip Angle

The increase of ΔS with flip angle at short echo times and concomitant short repetition times is consistent with the idea that the observed signal increase is directly influenced by changes in blood flow (*9, 15, 16*). At an echo time of 50 ms, however, we could not detect any increase of ΔS with flip angle, which suggests that inflow effects could possibly be neglected at this echo and repetition time, at least up to flip angles of 60°. This view seems to be confirmed by Thompson *et al.* (*14*), who even found a slight decrease of ΔS with increased flip angle. However, we also observed increased flow artifacts at higher flip angles, especially caused by larger visible vessels, which suggests that we nevertheless have to take into account the effects of increased flow. Duyn *et al.* (*16*) found significant inflow effects using FLASH with flip angles of 40°. In their study signal changes were considerably enhanced with a slice-selective inversion prepulse and suppressed with a global inversion prepulse or saturation slabs around the imaging slice. However, they did not study the dependence of the inflow effect on echo and repetition time. Frahm *et al.* (*15*) stated that inflow contrast is maximized at short TE (≤10 ms), short TR (≤70 ms), high flip angles (≥40°), and thin slices (≤4 mm) but they did not quantify concomitant signal increases. However, the time courses in visual cortex at long TE which are shown in their Fig. 3 do not indicate a considerable increase of ΔS with flip angle. According to the theoretical work of Gao *et al.* (*25*), who analyzed the influence of increased flow on the fMRI signal changes, there is a strong influence not only from the parameters of the imaging sequences mentioned above but also from the flow patterns, the initial baseline velocity, and the ratio of blood to gray matter within the pixel. They found that under certain circumstances inflow can also lead to a signal decrease. They conclude that, in combination with the BOLD effect, the inflow of blood can lead to an increase, as well as to a decrease, of the signal. This

means that the lack of an increase in ΔS does not necessarily imply the absence of inflow effects. Also, phase changes due to increased in-plane flow during activation lead to confounding signal changes which, according to them, could be diminished by application of flow compensating gradient waveforms in the phase and frequency encoding direction. It remains unclear whether the use of flow compensation in the readout and slice encoding direction always leads to a slightly diminished signal increase, as observed by us; this needs further investigation. Gao *et al.* (*25*) also stated that in conventional gradient echo pulse sequences the signal change due to inflow is dominant in cortical draining veins, whereas the inflow contribution in capillary areas is negligible. However, in larger vessels the T_2^* relaxation times can be considerably shorter (*8, 11*), which might cause a diminished inflow signal at longer echo times due to intravascular dephasing. On the other hand, draining venous vessels are also known for large susceptibility-induced signal changes (*3*), which might by far exceed the changes due to inflow. Probably these explanations all hold true in certain situations, which means that inflow can considerably confound results of functional imaging studies. Also taking the decrease in CNR^n_{pix} and N_{act} at higher flip angles into account, it is certainly favorable to use small flip angles lower than 30°.

Significance of SNR and CNR

Our results demonstrate that the quality of a fMRI experiment does not only depend on ΔS but also on the noise characteristic of the imaging experiment (*20*). In most cases, an increase in ΔS is accompanied by a decrease in SNR. This means that one has to choose a compromise where SNR is high enough and ΔS is still large enough to be detectable. A quantitative measure for this optimal parameter value is CNR^n or CNR^n_{pix}. The global CNR^n gives an upper limit for the contrast-to-noise ratio. It assumes that the baseline fluctuations are only due to random fluctuations of a constant noise level which can be determined by the SNR of the first image. Since this assumption is certainly not valid in real experimental situations, we preferred CNR^n_{pix}, since it takes into account the dynamic noise characteristic of the imaging sequences upon different parameter settings. This quantity is highly sensitive to any kind of instability in the pixel time course which can be due to system instabilities as well as artifacts (e.g., flow at higher FA) and physiological fluctuations. This means that optimization of SNR_{pix} is vital, since time-course stability is extremely important for the detection of small signal changes. For parameters which influence ΔS as well as SNR_{pix}, the optimal value is given by the maximum of CNR^n_{pix}. If only SNR_{pix} is influenced, the maxima of CNR^n_{pix} and SNR_{pix} coincide. We generally found that SNR_{pix}, and especially CNR^n_{pix}, was substantially lower than the global quantities SNR and CNR^n. It is obvious that SNR_{pix} has to be significantly smaller than SNR because of additional physiological fluctuations (*20*). Thomas and Menon (*20*) investigated the noise spectrum in EPI time series at different echo times; they found the noise to increase with echo time and also at least 30% of the total noise being due to cardiac and respiratory motion. In FLASH imaging, this motion occurs during the relatively long image acquisition period and leads to increased fluctuations in the image intensity, which might be reduced by the use of navigator echoes (*26*). However, CNR^n_{pix} is further diminished by another effect. Pixels with large signal changes often also show large fluctuations, since they are usually located at larger vessels, where pulsatile flow and phase shifts occur (*3*). This leads to a small CNR^n_{pix}, since the combination of large signal increase and fluctuations directly compensate each other because of pixelwise calculation. For calculation of CNR^n the opposite effect occurs: even a small number of large pixel values leads to an elevated mean value ΔS, while SNR is not influenced, which finally results in an elevated CNR^n. This shows that the CNR^n is overestimated if determined from the global SNR and ΔS. On the other hand, CNR^n_{pix} probably underestimates the true contrast-to-noise ratio, since the baseline time course in activated pixels certainly shows increased deviations in reaction to the stimulus. We tried to minimize this effect by discarding the first (two) data point(s) in each period, in order to avoid nonequilibrium effects, but there still remain contributions, e.g., due to the transient poststimulus undershoot which may be as large as the positive signal response to the stimulus (*22, 23*). Probably, these influences additionally vary with the imaging conditions. Nevertheless, the overall behavior of CNR^n_{pix} certainly yields useful clues for the determination of the optimal parameter values, since it is highly sensitive to any instability in the pixel time course. The global CNR^n, SNR, and the number of activated pixels provide additional information to avoid misinterpretations.

Acquisition Time and SNR

Although a low BW provides a good SNR, it also causes severe chemical shift artifacts and blurring. Thus it was not clear if the lowest BW would be the optimal value. Additionally, the prolonged acquisition time enhances the sensitivity to motion. Indeed, ΔS increased slightly toward a BW of 15 kHz, and CNR^n_{pix} showed a minimum at medium bandwidth. This behavior might suggest that the use of a higher BW could be favorable. However, the concomitant strong decrease of SNR, CNR^n, and N_{act} indicated an artifactual increase of ΔS, caused by the selective detection of high signal changes due to the low SNR at a BW of 15 kHz. This means that activation in pixels with low ΔS_{pix} disappears and that ΔS as well as CNR^n_{pix} is artificially elevated.

One reason for the superiority of a small BW is the long T_2^* in human brains at 2 T. Prolonged acquisition time improves SNR as long as there is still enough signal to detect. The expected optimum for the SNR lies at an acquisition time equal to $1.26 \cdot T_2^*$ (*27*). Consequently, high BW and concomitant short acquisition times usually used in FLASH imaging lead to

a significant loss in SNR, particularly in tissues with long T_2^*. This is one of the reasons why EPI is widely used in fMRI. At low resolution, EPI offers an acceptable image quality in large portions of the brain. Additionally, EPI offers intrinsic T_2^* weighting and very short image acquisition times, which highly diminish motion sensitivity in concert with the possibility of high volume coverage. However, in the lower parts of the brain, EPI suffers not only from signal loss but also from severe image distortions. This problem is particularly severe at higher field strengths. One possibility to overcome the limitations of both methods is to use a FLASH-EPI-Hybrid method, which on the one hand reduces susceptibility artifacts (*28*), and on the other hand also allows relatively fast acquisition of images with optimized SNR (*29, 30*). Hillenbrand *et al.* (*30*) recently verified that the SNR of a FLASH-EPI-Hybrid method can be optimized according to T_2^* by the use of an appropriate number of echoes per excitation, as well as an optimized flip angle. Compared to a FLASH image with the same bandwidth, an EPI-FLASH-Hybrid yields a gain in SNR as long as the acquisition time per excitation is not longer than $1.26 \cdot T_2^*$. The concomitant increase in repetition time also allows the use of higher flip angles, which additionally improves SNR (*29*). EPI-FLASH-Hybrid sequences have already been applied to fMRI (*19, 28*). Since the signal increase mainly depends on echo time, field strength, and spatial resolution, maximal CNR^n should be obtained, if, at optimal TE and spatial resolution, the flip angle and number of echoes are optimized for maximal SNR. However, care has to be taken to avoid specific artifacts and to diminish motion sensitivity through the use of navigator echoes (*28*).

Number of Activated Pixels

Generally, the number of activated pixels showed a large deviation over subjects in all experiments. This was probably due to interindividual variations as well as to limitations of this study. The length of the full experiment, and the fact that only one slice could be observed, probably led to several effects, which influenced the number of activated pixels. We observed that the number of activated pixels tended to decrease during sessions. This may be partly due to the fact that the basic sequence was already rather optimal. However, recessive attention, increasing drowsiness, and motion of the subjects probably also led to diminished activation. Motion could affect the results in several respects: While larger motions mainly occurred between experiments, and led to slight variations of the imaging plane, small motions during the experiments simply degraded the quality of the functional image. This session effect was partly counteracted by the individual splitting of the sessions which resulted in an irregular distribution of the breaks. In addition to this, the subjects were contacted several times during the sessions to maintain their attention. An even better elimination of session effects might be be achieved by a randomization of the paradigm; this will be done in further studies. However, parameters which systematically yielded a small N_{act}, such as high BW, short TE, and very small pixel size, are obviously inappropriate for reliable detection of activation. This is mainly due to very low SNR (high BW, small pixel size) or small ΔS (short TE).

CONCLUSION

The following parameter values were found to be optimal: An echo time of 40 to 50 ms, a rather low spatial resolution (ST $\approx$5 mm, pixel size $\approx$2.3–4.6 mm, matrix 64×48), and small flip angles lower than 30°. As FLASH methods, especially in single-slice mode, are prone to inflow effects, the latter also seems favorable because of additionally reduced inflow sensitivity. In terms of maximal CNR^n, flow compensation should not be applied as it slightly reduces ΔS. Furthermore, a rather low BW of 2.5 kHz is favorable in spite of some artifacts, since it yields superior SNR. Application of a phase rewinder increases SNR and improves the results slightly.

ACKNOWLEDGMENTS

The authors thank Dr. P. M. Jakob and Dr. E. Hofmann for helpful discussions.

REFERENCES

1. K. K. Kwong, J. W. Belliveau, D. A. Chesler, I. E. Goldberg, R. M. Weisskoff, B. P. Poncelet, D. N. Kennedy, B. E. Hoppel, M. S. Cohen, R. Turner, H.-M. Cheng, Th. J. Brady, and B. R. Rosen, Dynamic magnetic resonance imaging of human brain activity during primary sensory stimulation, *Proc. Natl. Acad. Sci. USA* **89,** 5675–5679 (1992).
2. S. Ogawa, D. W. Tank, R. Menon, J. M. Ellermann, S.-G. Kim, H. Merkle, and K. Ugurbil, Intrinsic signal changes accompanying sensory stimulation: Functional brain mapping with magnetic resonance imaging, *Proc. Natl. Acad. Sci. USA* **89,** 5951–5955 (1992).
3. E. M. Haake, A. Hopkins, S. Lai, P. Buckley, L. Friedman, H. Meltzer, P. Hedera, R. Friedland, S. Klein, L. Thompson, D. Detterman, J. Tkach, and J. S. Lewin, 2D and 3D high resolution gradient echo functional imaging of the brain: Venous contributions to signal in motor cortex studies, *NMR Biomed.* **7,** 54–62 (1994).
4. S. Ogawa, T. M. Lee, and B. Barrere, The sensitivity of magnetic resonance image signals of a rat brain to changes in the cerebral venous blood oxygenation, *Magn. Reson. Med.* **29,** 205–210 (1993).
5. S. Ogawa, R. S. Menon, D. W. Tank, S.-G. Kim, H. Merkle, J. M. Ellermann, and K. Ugurbil, Functional brain mapping by blood oxygenation level-dependent contrast magnetic resonance imaging: A comparison of signal characteristics with a biophysical model, *Biophys. J.* **64,** 803–812 (1993).
6. S. Ogawa, T. M. Lee, A. R. Kay, and D. W. Tank, Brain magnetic resonance imaging with contrast dependent on blood oxygenation, *Proc. Natl. Acad. Sci. USA* **87,** 9868–9872 (1990).
7. P. T. Fox and M. E. Raichle, Focal physiological uncoupling of cerebral blood flow and oxidative metabolism during somatosensory stimulation in human subjects, *Proc. Natl. Acad. Sci. USA* **83,** 1140–1144 (1986).

8. R. S. Menon, S. Ogawa, D. W. Tank, and K. Ugurbil, 4 Tesla gradient recalled echo characteristics of photic stimulation-induced signal changes in the human primary visual cortex, *Magn. Reson. Med.* **30,** 380–386 (1993).
9. S. G. Kim, K. Hendrich, X. Hu, H. Merkle, and K. Ugurbil, Potential pitfalls of functional MRI using conventional gradient recalled echo techniques, *NMR Biomed.* **7,** 69–74 (1994).
10. R. Turner, R. Jezzard, H. Wen, K. K. Kwong, D. Le Bihan, T. Zeffiro, and R. S. Balaban, Functional mapping of the human visual cortex at 4 and 1.5 Tesla using deoxygenation contrast EPI, *Magn. Reson. Med.* **29,** 277–279 (1993).
11. J. S. Gati, R. S. Menon, K. Ugurbil, and B. K. Rutt, Experimental determination of the BOLD field strength dependence in vessels and tissue, *Magn. Reson. Med.* **38,** 296–302 (1997).
12. J. Frahm, K.-D. Merboldt, and W. Hänicke, Functional MRI of human brain activation at high spatial resolution, *Magn. Reson. Med.* **29,** 139–144 (1993).
13. S. Lai, L. Hopkins, E. M. Haake, D. Li, B. A. Wasserman, P. Buckley, L. Friedman, H. Meltzer, P. Hedera, and R. Friedland, Identification of vascular structures as a major source of signal contrast in high resolution 2D and 3D functional activation imaging of the motor cortex at 1.5 T: Preliminary results, *Magn. Reson. Med.* **30,** 387–402 (1993).
14. R. M. Thompson, C. R. Jack, K. Butts, D. P. Hanson, S. J. Riederer, R. L. Ehman, R. W. Hynes, and N. J. Hangiandreou, Imaging of cerebral activation at 1.5 T: Optimizing a technique for conventional hardware, *Radiology* **190,** 873–877 (1994).
15. J. Frahm, K.-D. Merboldt, W. Hänicke, A. Kleinschmidt, and H. Boecker, Brain or vein—Oxygenation or flow? On signal physiology in functional MRI of human brain activation, *NMR Biomed.* **7,** 45–53 (1994).
16. J. H. Duyn, C. T. W. Moonen, G. H. van Yperen, R. W. de Boer, and P. R. Luyten, Inflow versus deoxyhemoglobin effects in BOLD functional MRI using gradient echoes at 1.5 T, *NMR Biomed.* **7,** 83–88 (1994).
17. R. S. Menon, S. Ogawa, X. Hu, J. P. Strupp, P. Anderson, and K. Ugurbil, BOLD based functional MRI at 4 Tesla includes a capillary bed contribution: Echo-planar imaging correlates with previous optical imaging using intrinsic signals, *Magn. Reson. Med.* **33,** 453–459 (1995).
18. A. T. Lee, G. H. Glover, and C. H. Meyer, Discrimination of large venous vessels in time-course spiral blood-oxygen-level-dependent magnetic-resonance functional neuroimaging, *Magn. Reson. Med.* **33,** 745–754 (1995).
19. R. S. Menon, C. G. Thomas, and J. S. Gati, Investigation of BOLD contrast in fMRI using multi-shot EPI, *NMR Biomed.* **10,** 179–182 (1997).
20. C. G. Thomas and R. S. Menon, Amplitude response and stimulus presentation frequency response of human primary visual cortex using BOLD EPI at 4 T, *Magn. Reson. Med.* **40,** 203–209 (1998).
21. P. T. Fox, and M. E. Raichle, Stimulus rate dependence of regional cerebral blood flow in human striate cortex demonstrated by positron emission tomography, *J. Neurophysiol.* **51**(5), 1109–1120 (1984).
22. W. Chen, X. H. Zhu, T. Kato, P. Andersen, and K. Ugurbil, Spatial and temporal differentiation of fMRI BOLD response in primary visual cortex of human brain during sustained visual stimulation, *Magn. Reson. Med.* **39,** 520–527 (1998).
23. R. B. Buxton, E. C. Wong, and L. R. Frank, Dynamics of blood flow and oxygenation changes during brain activation: The balloon model, *Magn. Reson. Med.* **39,** 855–864 (1998).
24. L. Kaufman, D. M. Kramer, L. E. Crooks, and D. A. Ortendahl, Measuring signal-to-noise ratios in MR imaging, *Radiology* **173,** 265–267 (1989).
25. J.-H. Gao, I. Miller, S. Lai, J. Xiong, and P. T. Fox, Quantitative assessment of blood inflow effects in functional MRI Signals, *Magn. Reson. Med.* **36,** 314–319 (1996).
26. X. Hu and S.-G. Kim, Reduction of signal fluctuations in functional MRI using navigator echoes, *Magn. Reson. Med.* **31,** 495–503 (1994).
27. R. Pohmann, M. von Kienlin, and A. Haase, Theoretical evaluation and comparison of fast chemical shift imaging methods, *J. Magn. Reson.* **129,** 145–160 (1997).
28. S.-G. Kim, X. Hu, and K. Ugurbil, Fast interleaved echo-planar imaging with navigator: High resolution anatomic and functional images at 4 Tesla, *Magn. Reson. Med.* **35,** 895–902 (1996).
29. R. Deichmann, H. Adolf, U. Nöth, E. Kuchenbrodt, C. Schwarzbauer, and A. Haase, Calculation of signal intensities in hybrid sequences for fast NMR imaging, *Magn. Reson. Med.* **34,** 481–489 (1995).
30. C. Hillenbrand, R. Deichmann, D. Hahn, and A. Haase, Signal intensities in FLASH-EPI-Hybrid sequences, *J. Magn. Reson.* **139,** 74–80 (1999).